Meteorological characteristics of ~~extreme~~severe ozone pollution events in China and their future predictions

Yang Yang[1*], Yang Zhou[2], Hailong Wang[3], Mengyun Li[1], Huimin Li[1], Pinya Wang[1], Xu Yue[1],

Ke Li[1], Jia Zhu[1], Hong Liao[1]

[1]Joint International Research Laboratory of Climate and Environment Change, Jiangsu Key

Laboratory of Atmospheric Environment Monitoring and Pollution Control, Jiangsu

Collaborative Innovation Center of Atmospheric Environment and Equipment Technology,

School of Environmental Science and Engineering, Nanjing University of Information

Science and Technology, Nanjing, Jiangsu, China

[2]Shanghai Baoshan Meteorology Bureau, Shanghai, China

[3]Atmospheric Sciences and Global Change Division, Pacific Northwest National Laboratory,

Richland, WA, USA

*Correspondence to yang.yang@nuist.edu.cn

Abstract

Ozone (O_3) has become one of the most concerning air pollutants in China in recent decades. In this study, based on surface observations, reanalysis data, global atmospheric chemistry model simulations and multi-model future predictions, meteorological characteristics conducive to extremesevere O_3 pollution in various regions of China are investigated, and their historical changes and future trends are analyzed. During the most severe O_3 polluted months, the chemical production of O_3 is enhanced under the hot and dry conditions over the North China Plain (NCP) in June 2018 and Yangtze River Delta (YRD) in July 2017, while the regional transport is the main reason causing the severe O_3 pollution over Sichuan Basin (SCB) in July 2015 and Pearl River Delta (PRD) in September 2019. Over the last four decades, the frequencies of high temperature and low relative humidity conditions increased in 2000-2019 relative to 1980-1999, indicating that O_3 pollution in both NCP and YRD became more frequent under the historical climate change. In SCB and PRD, the occurrence of atmospheric circulation patterns similar to those during the most polluted months increased, together with the more frequent hot and dry conditions, contributing to the increases in severe O_3 pollution in SCB and PRD during 1980–2019. In the future (by 2100), the frequencies of months with anomalous high temperature show stronger increasing trends in the high forcing scenario (SSP5-8.5) compared to the sustainable scenario (SSP1-2.6) in China. It suggests that high anthropogenic forcing will not only lead to slow economic growth and climate warming, but also likely result in environmental pollution issues.

1. Introduction

Tropospheric ozone (O_3), one major air pollutant, is formed in photochemical reactions of nitrogen oxides (NO_x) and volatile organic compounds (VOCs) when exposed to sunlight (Finlayson-Pitts and Pitts, 1997; Silman, 1999). Enhanced O_3 pollution harms ecosystems and human health (Fleming et al., 2018; Maji et al., 2019) by reducing crop yields (Ainsworth et al., 2012; Mills et al., 2018) and aggravating cardiopulmonary disease (Ebi and McGregor, 2008; Liu et al. 2018). In recent years, near-surface ozone concentrations in many regions of China have been increasing considerably (Verstraeten et al., 2015; Cheng et al., 2019; Zhang et al., 2020, Li et al., 2019; Lu et al., 2018; Silver et al., 2018; Yin et al., 2019, Lu et al., 2020). Lu et al. (2020) revealed that the daily maximum of 8-h average O_3 concentration (MDA8-O_3) in China increased by 2.4 ppb per year (5.0% relative to the average) during April–September over 2013–2019.

In addition to emissions, O_3 concentrations are influenced by meteorological factors such as temperature, relative humidity, solar radiation, and winds (Mott et al., 2005; Fu and Tian, 2019; Gong and Liao, 2019; Li et al., 2019, 2020; Le et al., 2020; Zhao et al., 2020). Typically, strong solar radiation, high surface air temperatures, and low relative humidity are conducive to photochemical production of O_3, causing a raise of O_3 concentration (Peterson and Flowers, 1977; Xu, et al., 2011; Coates et al., 2016; Li et al., 2020; Dang et al., 2021). Wind speed is negatively correlated with surface O_3 because low wind speed facilitates the accumulation of O_3 upon production (Zhang et al., 2015; Wang et al., 2017; Liu and Wang, 2020). Han et al. (2020) explored the impacts of various meteorological factors on the daily variation of summer surface O_3 in eastern China based on a multiple linear regression method and suggested that

65 relative humidity is the primary factor affecting O_3 concentration in central and south parts of

66 eastern China, while temperature is the most important factor governing O_3 concentration in

67 north of eastern China. Gong and Liao (2019) reported that the meteorological characteristics

68 of O_3 pollution events in North China during 2014–2017 were the high daily maximum

69 temperature, low relative humidity, abnormal southerly winds and high pressure at 500 hPa.

70 These findings emphasize that meteorological factors play a crucial role in regulating O_3

71 pollution in China.

72 Atmospheric circulation patterns affect O_3 concentrations over China through changing

73 meteorological factors (Yang et al, 2014, 2022; Zhao and Wang, 2017; Shu et al., 2019; Dong

74 et al., 2020; Zhou et al., 2022). Zhao and Wang (2017) examined the influence of the Western

75 Pacific Subtropical high (WPSH) on O_3 over eastern China based on observations and

76 reanalysis data from 2014 to 2016. They found that stronger WPSH enhanced the moisture

77 transport to southern China, which was detrimental to the photochemical reaction of O_3,

78 leading to a decrease in surface O_3 concentration in southern China, whereas O_3 concentrations

79 in northern China increased under the stronger WPSH related to the dry and hot conditions

80 favoring O_3 production. On the basis of observational O_3 data and ERA5 reanalysis data during

81 2014–2018, Dong et al. (2019) analyzed the impact of synoptic patterns on summertime O_3

82 pollution in the North China Plain and revealed that the most severe O_3 pollution weather

83 pattern is associated with anomalous southwesterly winds, which carry dry, warm air from

84 inland southern China to the North China Plain and favor the chemical production of O_3. Zhou

85 et al. (2022) explored the impacts of Asian summer monsoon on the interannual variation of

86 O_3 concentrations based on surface measurements and GEOS-Chem model simulations. They

87   showed that the East Asian summer monsoon strength was positively correlated with O_3

88   concentration in south-central China and South Asian summer monsoon has complex effects

89   on O_3 pollution in China, mainly through changing transboundary transport related to large-

90   scale circulations.

91   As mentioned above, many previous studies have examined the meteorological

92   characteristics of O_3 pollution in China. However, they focused on O_3 pollution over limited

93   regions in China in each study (e.g., the North China Plain, southern China). These studies only

94   examined the meteorological characteristics of O_3 pollution in a short time period due to the

95   lack of observational data and did not consider the historical and future trends of these

96   meteorological factors. In this study, the meteorological characteristics conducive to the most

97   severe O_3 pollution in several polluted areas of China, including the North China Plain (NCP),

98   Yangtze River Delta (YRD), Sichuan Basin (SCB), and Pearl River Delta (PRD), are

99   respectively investigated based on the observed surface O_3 concentrations, reanalysis data, and

100   GEOS-Chem model simulations. Besides, the contributions from various chemical and

101   physical processes inducing regional O_3 pollution are quantified using an integrated process

102   rate (IPR) analysis method. The historical changes in these meteorological factors favoring the

103   most severe O_3 pollution over 1980–2019 are provided. Moreover, variations in future

104   meteorological patterns during 2021–2100 leading to severe O_3 pollution in China are

105   presented under the sustainable and high forcing scenarios according to the multi-model data

106   from the Coupled Model Intercomparison Project Phase 6 (CMIP6).

107   **2. Methods**

108   **2.1 Surface ozone observations and meteorological reanalysis**

109   Hourly surface O_3 concentrations are obtained from the Ministry of Ecology and

110   Environment (MEE) of China. The observational network was established in 2013 with 450

111   monitoring sites and increased to 1,500 monitoring sites by 2019, covering about 360 cities in

112   China. MDA8-O_3 are calculated based on hourly O_3 concentrations from April-September

113   during 2013 to 2020. In this study, O_3 pollution days are defined as the days when MDA8-O_3

114   exceeds 160 μg m^{-3} according to the China National Ambient Air Quality Standard (GB3095-

115   2012).

116   The meteorological fields are taken from the European Centre for Medium-Range

117   Weather Forecasts (ECMWF) ERA5 monthly reanalysis dataset during 1980–2020, with a

118   horizontal resolution of 0.25° × 0.25°. To explore the meteorological characteristics that are

119   conducive to O_3 pollution, sea level pressure (SLP), geopotential height (GPH) at 500 hPa,

120   wind fields at 850 hPa and 500 hPa, temperature at 2m (T2m) and surface relative humidity

121   (RH) are adopted, which can have significant impacts on O_3 variations in China (Jiang et al.,

122   2020; Dong et al., 2020; Le et al., 2020).

2.2 GEOS-Chem model simulations

124   O_3 concentrations and the related chemical and physical processes causing O_3 variations

125   over 1981–2020 are simulated in the global atmospheric chemistry model GEOS-Chem

126   (version V12.9.3), driven by the Modern-Era Retrospective analysis for Research and

127   Application, Version 2 (MERRA-2). Simulations are performed on 47 vertical layers from

128   surface to 0.01 hPa, and a horizontal grid of 2° latitude × 2.5° longitude. GEOS-Chem model

129   incorporates a fully coupled O_3-NO_x-hydrocarbon-aerosol chemical mechanism (Pye et al.,

130   2009; Mao et al., 2013; Sherwen et al., 2016). Boundary-layer mixing uses a non-local scheme

131   (Lin and McElroy, 2010), and stratospheric O_3 chemistry employs the linearized O_3

132   parameterization (LINOZ) (McLinden et al., 2000).

133   Global anthropogenic ~~aerosol and precursor gas~~ emissions driving the simulations are

134   from the Community Emissions Data System (CEDS, Hoesly et al., 2018) and biomass burning

135   emissions are from the Global Fire Emissions Database, Edition 4 (GFED4, Van der Werf et

136   al., 2017). VOCs emissions from biogenic sources are provided offline by the Model of

137   Emissions of Gases and Aerosols from Nature version 2.1 (MEGAN V2.1, Guenther et al.,

138   2012). Lightning and soil emissions are specified in the model (Hudman et al., 2012; Ott et al.,

139   2010). Anthropogenic emissions in China are updated with the Multi-resolution Emission

140   Inventory (MEIC), a localized emission dataset for China. Anthropogenic, biomass burning,

141   ~~biological~~ biogenic and other natural emissions are kept at 2017 levels during the simulations,

142   so as to eliminate the influence of emission changes on the interannual variation and trends of

143   O_3. Simulated O_3 distributions with the same configuration in GEOS-Chem have been

144   extensively evaluated in many studies, and the model has been reported to capture O_3

145   concentrations well in China (e.g., Li et al., 2019; Lu et al., 2019; Ni et al., 2018).

146 2.3 CMIP6 multi-model simulations

147   The multi-model simulations from historical and the Scenario Model Intercomparison

148   Project (ScenarioMIP) in CMIP6 are used to analyze the historical variations and future trends

149   of meteorological conditions conducive to the most severe O_3 pollution. Two different future

150   scenarios of the Shared Socioeconomic Path (SSPs) are applied, including the sustainable

151   scenario (SSP1-2.6) and the high forcing scenario (SSP5-8.5). Totally simulations from 13

152   models (ACCESS-CM2, ACCESS-ESM1-5, CAS-ESM2-0, CMCC-CM2-SR5, CMCC-ESM2,

153 FGOALS-f3-L, FGOALS-g3, GFDL-ESM4, INM-CM4-8, INM-CM5-0, IPSL-CM6A-LR,

154 MPI-ESM1-2-HR, MPI-ESM1-2-LR) are analyzed in this study.

3. Results

3.1 Meteorological characteristics conductive to regional ozone pollution

157   To investigate the relationship between meteorological conditions and regional O_3

158 pollution in China, the frequencies of O_3 pollution days from April to October during 2013–

159 2020 are calculated for Beijing, Shanghai, Chengdu and Guangzhou, representing the typical

160 four polluted regions in China (i.e., NCP, YRD, SCB and PRD) (Figure 1). Observational data

161 show the highest frequencies of O_3 pollution days in June 2018, July 2017 and September 2019

162 in Beijing, Shanghai and Guangzhou, with pollution days up to 22, 20 and 19 days per month,

163 respectively. The top three highest frequencies of O_3 pollution days in Chengdu are in July

164 2016, July 2015 and July 2018 (16, 15 and 15 days per month, respectively). Variations in O_3

165 concentration in the real world are driven by changes in both meteorological factors and

166 emissions. With fixed emissions, the positive anomalies of near-surface O_3 concentrations over

167 NCP, YRD and PRD during their most polluted months can also be reproduced by the GEOS-

168 Chem model (Figure 2), suggesting that the O_3 pollutions during the most polluted months over

169 NCP, YRD and PRD are likely attributable to the anomalies of meteorological conditions. In

170 the top three O_3 polluted months in Chengdu, only in July 2015 the higher concentrations than

171 the long-term averages can be captured by the simulations with fixed emissions. Therefore, in

172 this study, we focus on the meteorological characteristics in June 2018, July 2017, July 2015

173 and September 2019, that were conducive to the most severe O_3 pollution over NCP, YRD,

174 SCB and PRD, respectively.

175   When O_3 pollution was the most severe over NCP in June 2018, an anomalous high

176   pressure occurred at 500 hPa over NCP (Fig. 3b), relative to the 40-year climatological

177   averages from 1980 to 2019, leading to positive T2m anomalies near the surface (Fig. 3c).

178   Anomalous lows located over northeastern China and northwestern Pacific (Fig. 3a) and the

179   associated anomalous northerly winds prevent the moisture moving from the ocean to NCP,

180   causing negative RH anomalies over NCP (Fig. 3d). The meteorological conditions with the

181   high T2m and low RH are favorable for the photochemical production of O_3. When the most

182   severe O_3 pollution occurred in July 2017, YRD was dominated by anomalous high pressure

183   in the lower and middle troposphere (Figs. 4a and 4b). Under the control of high pressure, the

184   meteorological conditions (e.g., high T2m and low RH) enhance the photochemical production

185   of O_3 (Figs. 4c and 4d). In the O_3 pollution event of SCB in July 2015, the negative T2m

186   anomaly is not conducive to the O_3 production (Fig. 5c), although the RH was low (Fig. 5d).

187   Meanwhile, the anomalous low over eastern China and northwestern Pacific in the middle

188   troposphere favors regional O_3 transport from the polluted source region over eastern China to

189   SCB (Fig. 5b) and the anomalous high over central-western China is conducive to the vertical

190   transport of upper tropospheric O_3 down to the lower troposphere (Fig. 5a). For the PRD in

191   September 2019, the anomalous high covering almost the entire China along with the

192   anomalous low over East China Sea generates northerly wind anomalies in the lower

193   troposphere over eastern China, which tend to transport polluted air from northern China and

194   weaken the inflow of oceanic clean air (Fig. 6). The temperature increase is much more

195   significant in the upwind regions as compared to PRD, suggesting that the strong regional

196   transport could be the primary reason causing this severe O_3 pollution event of PRD.

3.2 Physical and chemical mechanisms leading to regional ozone pollution

To further explore the mechanisms of meteorological changes leading to the severe O_3 pollution over the four typical polluted regions in China, contributions of individual chemical and physical processes to O_3 variations are quantified based on the IPR analysis from GEOS-Chem simulations and summarized in Table 1.

Consistent with the meteorological anomalies analyzed above, high temperature and low RH meteorological conditions in NCP are conducive to the photochemical production of O_3. During the polluted month over NCP, the chemical production of tropospheric O_3 is higher than the long-term average by 2.36 Gg day^{-1}, while the horizontal transport also contributes to the increase in O_3 mass by 1.58 Gg day^{-1} (Table 1). Due to the enhanced northwesterly winds, the import of O_3 mass from the north and west of NCP was increased by 1.80 and 0.62 Tg, respectively (Table 2). In YRD, the chemical production (2.38 Gg day^{-1}) is also the dominant process that drives the O_3 concentration increase during the most severe polluted month, associated with the warm and dry conditions. Therefore, the anomalous chemical production is the major process that induced O_3 pollution in NCP and YRD during the most severe polluted months.

Different from NCP and YRD, horizontal transport is the main process that caused O_3 pollution in SCB and PRD during the most severe ~~polluted~~ months. It contributes to the rate of increase in O_3 mass by 5.10 and 6.67 Gg day^{-1}, respectively, over SCB and PRD, while other processes tend to decrease the O_3 mass (Table 1). Due to the anomalous northerly winds over SCB, more O_3 is transported into SCB from north (by 4.02 Tg), and the anomalous northeasterly winds enhance the O_3 transport from the north and east of PRD by 1.97 and 1.09

219 Tg, respectively, leading to the increase in O_3 concentrations over SCB and PRD during the

220 most severe ~~polluted~~ months relative to the climatological averages (Table 2). Note that, the

221 chemical production of tropospheric O_3 decreased in SCB and PRD during the most severe

222 ~~polluted~~ months. It could have been biased by the relatively coarse model resolution in this

223 study (2° latitude × 2.5° longitude), since that the SCB and PRD for calculating the chemical

224 and physical processes only cover limited grid boxes. Further studies should be performed

225 using a model with finer resolution or a nested simulation method.

3.3 Historical and future changes in the meteorological conditions

227   O_3 pollution has deteriorated in China during recent decades, which could be related to

228 the changes in meteorological conditions. Time series of T2m and RH anomalies in the polluted

229 months during the 1980–2019 and frequencies of high T2m and low RH months during 1980–

230 1999 and 2000–2019 over the four polluted regions in China based on ERA5 reanalysis data

231 are shown in Figure 7. Due to climate change, both the high temperature and low RH conditions

232 in NCP, YRD, SCB and PRD all increased during the past four decades (2000-2019 versus

233 1980-1999). Based on the analysis showing that chemical production is the dominant process

234 of the most severe O_3 pollution in NCP and YRD, the increases in the frequency of high

235 temperature and low RH indicate that severe O_3 pollution in both NCP and YRD has become

236 more frequent under the historical climate change. In SCB and PRD, the most severe O_3

237 pollution is more related to changes in regional transport. Similar to the analyzing method used

238 in previous studies (Li et al., 2018; Yang et al., 2021), the SLP and 500 hPa GPH over East

239 Asia and Western Pacific in the same month of each year similar to those during the most severe

240 ~~polluted~~ months in both SCB and PRD have increased (2000-2019 versus 1980-1999) (Figure

8), together with the more frequent hot and dry conditions (Figure 7), leading to the increases

in severe O_3 pollution in SCB and PRD during 1980–2019.

Many studies have reported that future climate change will have significant influences

on O_3 pollution in China through changing meteorological factors (e.g., Li et al., 2023; Wang

et al., 2022). Here, the frequencies of extreme months with high T2m and low RH and the

frequencies of extreme months with SLP and 500 hPa GPH that have moderate to high

correlation to those in the most polluted months in the four regions of China, under the

sustainable (SSP1-2.6) and high forcing (SSP5-8.5) scenarios during 2021–2100 from CMIP6

multi-model results, are presented in Figures 9 and 10, respectively. Unlike the historical

changes in the meteorological conditions that caused the severe O_3 pollution through chemical

production and regional transport, future variations in meteorological conditions conducive to

the severe O_3 pollution are more related to the global warming process that enhances the O_3

production in China. The frequencies of months with anomalous high temperature show

obvious upward trends in both SSP1-2.6 and SSP5-8.5 scenarios over the four regions, and the

increasing trends in SSP5-8.5 are much more significant than in SSP1-2.6. Frequencies of low

RH months show downward trends in NCP, YRD and SCB, especially under SSP5-8.5, while

there is an upward trend in PRD. Note that the trends in frequencies of low RH months are

much less significant than in high temperature months. The frequencies of extreme months

with SLP and 500 hPa GPH that are similar to those in the most severe O_3 pollution months in

the four regions do not show significant trends in the SSPs. Hence, the future climate change

may aggregate O_3 pollution in China by enhancing the chemical production related to

temperature increases. The O_3 pollution exacerbation is projected to be less significant in the

263 sustainable scenario due to the moderate temperature increase than in the high forcing scenario,

264 suggesting that the sustainable scenario is the optimal path to retaining clean air in China. High

265 anthropogenic radiative forcing will not only lead to slow economic growth and climate

266 warming, but also result in the environmental pollution.

4. Conclusions and Discussions

268 O_3 pollution harms ecosystems and human health. In recent years, near-surface O_3

269 concentrations in many regions of China have been increasing considerably. Base on

270 observational O_3 data, ERA5 reanalysis data and GEOS-Chem model simulations,

271 meteorological characteristics conducive to extremesevere O_3 pollution in different regions of

272 China are investigated in this study. Contributions from various chemical and physical

273 processes inducing O_3 pollution are quantified using the an integrated process rate (IPR)

274 analysis method. Furthermore, historical changes and future trends of meteorological

275 conditions leading to severe O_3 pollution in China are explored based on the meteorological

276 reanalysis and CMIP6 multi-model future predictions, which is of great implication for the

277 mitigation and prevention of O_3 pollution over China.

278 In this study, June 2018, July 2017, July 2015 and September 2019 are identified as the

279 most severe O_3 pollution months influenced by meteorological factors over NCP, YRD, SCB

280 and PRD, respectively. Severe O_3 pollution in June 2018 over NCP and in July 2017 over YRD

281 is mainly due to enhanced chemical production related to hot and dry conditions. The chemical

282 production of O_3 in the most severe polluted months over NCP and YRD are 2.36 Gg day^{-1} and

283 2.38 Gg day^{-1}, respectively, higher than the climatological averages. Different from NCP and

284 YRD, regional transport is the main process leading to the high O_3 concentration in SCB and

285   PRD during the respective severely polluted months, which contributes to the rate of increase

286   in O_3 mass by 5.10 and 6.67 Gg day^{-1}, respectively, over SCB and PRD. During the most

287   severely polluted months, related to large-scale circulation patterns, anomalous northerly winds

288   transport more O_3 into SCB from north, and anomalous northeasterly winds enhance the O_3

289   transport from the north and east into PRD.

290   Over the last four decades (2000-2019 versus 1980-1999), the frequencies of high

291   temperature and low RH increased, indicating that O_3 pollution in both NCP and YRD has

292   become more frequent under the historical climate change. In SCB and PRD, the occurrence

293   of atmospheric circulation patterns similar to those during the most polluted months in both

294   SCB and PRD has increased, together with the more frequent hot and dry conditions, leading

295   to the increases in severe O_3 pollution in SCB and PRD during 1980–2019. In the future (by

296   2100), the frequencies of months with anomalous high temperature show obvious upward

297   trends in both sustainable (SSP1-2.6) and high forcing (SSP5-8.5) scenarios over the four

298   regions, and the increasing trends in SSP5-8.5 are much more significant than in SSP1-2.6.

299   This suggests that high anthropogenic radiative forcing will not only lead to slow economic

300   growth and climate warming, but also likely result in environmental pollution issues. The

301   sustainable scenario is the optimal path to retaining clean air in China.

302   There are some limitations and uncertainties in this work that can be further addressed in

303   future studies. For example, the model only captures the high O_3 concentrations in July 2015

304   in Chengdu among its top three polluted months. It is probably because the emissions are kept

305   at 2017 levels during the simulations. The high O_3 anomalies in July 2016 and July 2018 are

306   more likely influenced by the interannual changes in local precursor emissions in the

307   background of country-level increases in O_3 concentration in recent years. However, we also

308   can not rule out the possible inaccuracy in the model simulations to interpret severe O_3

309   pollution events in the SCB, which deserves further investigation with multi-model simulations.

310   In addition, this study focuses on the most extreme O_3 pollution in several polluted areas of

311   China. However, many other meteorological conditions can also cause O_3 pollution, although

312   they may not be as extreme as the cases analyzed in this study, which requires comprehensive

313   analysis for individual regions in future studies. Although the historical changes in the

314   meteorological patterns causing severe O_3 pollution are in accordance with the elevated O_3

315   levels in China in the recent decade, the quantitative analysis of meteorological impacts needs

316   full consideration of factors leading to O_3 pollution, including changes in anthropogenic and

317   natural emissions of its precursors, O_3 chemical regime, other meteorological factors conducive

318   to O_3 pollution, and stratosphere-troposphere exchange.

319

References

Ainsworth, E. A., Yendrek, C. R., Sitch, S., Collins, W. J., and Emberson, L. D.: The Effects of Tropospheric Ozone on Net Primary Productivity and Implications for Climate Change, Annu. Rev. Plant Biol., 63, 637-661, https://doi.org/10.1146/annurev-arplant-042110-103829, 2012.

Cheng, N., Li, R., Xu, C., Chen, Z., Chen, D., Meng, F., Cheng, B., Ma, Z., Zhuang, Y., He, B., and Gao, B.: Ground ozone variations at an urban and a rural station in Beijing from 2006 to 2017: trend, meteorological influences and formation regimes, J. Clean. Prod., 235, 11–20, https://doi.org/10.1016/j.jclepro.2019.06.204, 2019.

Coates, J., Mar, K. A., Ojha, N., and Butler, T. M.: The influence of temperature on ozone production under varying NOx conditions–a modelling study, Atmos. Chem. Phys., 16, 11601-11615, https://doi.org/10.5194/acp-16-11601-2016, 2016.

Dang, R., Liao, H., and Fu, Y.: Quantifying the anthropogenic and meteorological influences on summertime surface ozone in China over 2012-2017, Sci. Total Environ., 754, 142394, https://doi.org/10.1016/j.scitotenv.2020.142394, 2021.

Dong, Y., Li, J., Guo, J., Jiang, Z., Chu, Y., Chang, L., Yang, Y., and Liao, H.: The impact of synoptic patterns on summertime ozone pollution in the North China Plain, Sci. Total Environ., 735, 139559, https://doi.org/10.1016/j.scitotenv.2020.139559, 2020.

Ebi, K. L. and McGregor, G.: Climate change, tropospheric O_3 and particulate matter, and health impacts, Environ. Health Perspect., 116, 1449-1455, https://doi.org/10.1289/ehp.11463, 2008.

Finlayson-Pitts, B. J., and Pitts, J. N.: Tropospheric air pollution: Ozone, airborne toxics, polycyclic aromatic hydrocarbons, and particles, Science, 276, 1045-1052, https://doi.org/10.1126/science.276.5315.1045, 1997.

Fleming, Z. L., Doherty, R. M., Von Schneidemesser, E., Malley, C. S., Cooper, O. R., Pinto, J. P., Colette, A., Xu, X. B., Simpson, D., Schultz, M. G., Lefohn, A. S., Hamad, S., Moolla, R., Solberg, S., and Feng, Z. Z.: Tropospheric Ozone Assessment Report: Present-day ozone distribution and trends relevant to human health, Elementa-Sci. Anthrop., 6, 12, https://doi.org/10.1525/elementa.273, 2018.

Fu, T.-M., and Tian, H.: Climate change penalty to ozone air quality: Review of current understandings and knowledge gaps, Curr. Pollution Rep., 5, 159−171, https://doi.org/10.1007/s40726-019-00115-6, 2019.

Guenther, A. B., Jiang, X., Heald, C. L., Sakulyanontvittaya, T., Duhl, T., Emmons, L. K., and Wang, X.: The Model of Emissions of Gases and Aerosols from Nature version 2.1 (MEGAN2.1): an extended and updated framework for modeling biogenic emissions,

Geosci. Model Dev., 5, 1471–1492, https://doi.org/10.5194/gmd-5-1471-2012, 2012.

Gong, C., and Liao, H.: A typical weather pattern for ozone pollution events in North China, Atmos. Chem. Phys., 19, 13725−13740, https://doi.org/10.5194/acp-19-13725-2019, 2019.

Han, H., Liu, J., Shu, L., Wang, T. J., and Yuan, H.: Local and synoptic meteorological influences on daily variability in summertime surface ozone in eastern China, Atmos. Chem. Phys., 20, 203–222, https://doi.org/10.5194/acp-20-203-2020, 2020.

Hoesly, R. M., Smith, S. J., Feng, L., Klimont, Z., Janssens-Maenhout, G., Pitkanen, T., Seibert, J. J., Vu, L., Andres, R. J., Bolt, R. M., Bond, T. C., Dawidowski, L., Kholod, N., Kurokawa, J. I., Li, M., Liu, L., Lu, Z., Moura, M. C. P., O'Rourke, P. R., and Zhang, Q.: Historical (1750–2014) anthropogenic emissions of reactive gases and aerosols from the Community Emissions Data System (CEDS), Geosci. Model Dev., 11, 369–408, https://doi.org/10.5194/gmd-11-369-2018, 2018.

Hudman, R. C., Moore, N. E., Mebust, A. K., Martin, R. V., Russell, A. R., Valin, L. C., and Cohen, R. C.: Steps towards a mechanistic model of global soil nitric oxide emissions: implementation and space based-constraints, Atmos. Chem. Phys., 12, 7779–7795, https://doi.org/10.5194/acp-12-7779-2012, 2012.

Jiang, Z., Li, J., Lu, X., Gong, C., Zhang, L., and Liao, H.: Impact of western Pacific subtropical high on ozone pollution over eastern China, Atmos. Chem. Phys., 21, 2601–2613, https://doi.org/10.5194/acp-21-2601-2021, 2021.

Le, T., Wang, Y., Liu, L., Yang, J., Yung, Y., Li, G., and Seinfeld, J. H.: Unexpected air pollution with marked emission reductions during the COVID-19 outbreak in China, Science, 369, 702−706, https://doi.org/10.1126/science.abb7431, 2020.

Li, H., Yang, Y., Jin, J., Wang, H., Li, K., Wang, P., and Liao, H.: Climate-driven deterioration of future ozone pollution in Asia predicted by machine learning with multi-source data, Atmos. Chem. Phys., 23, 1131–1145, https://doi.org/10.5194/acp-23-1131-2023, 2023.

Li, K., Liao, H., Cai, W., and Yang, Y.: Attribution of anthropogenic influence on atmospheric patterns conducive to recent most severe haze over eastern China, Geophys. Res. Lett., 45, 2072–2081, https://doi.org/10.1002/2017gl076570, 2018.

Li, K., Jacob, D. J., Liao, H., Shen, L., Zhang, Q., and Bates, K. H.: Anthropogenic drivers of 2013–2017 trends in summer surface ozone in China, P. Natl. Acad. Sci. USA, 116, 422–427, https://doi.org/10.1073/pnas.1812168116, 2019.

Li, K., Jacob, D. J., Shen, L., Lu, X., De Smedt, I., and Liao, H.: Increases in surface ozone pollution in China from 2013 to 2019: anthropogenic and meteorological influences,

Atmos. Chem. Phys., 20, 11423–11433, https://doi.org/10.5194/acp-20-11423-2020, 2020.

Lin, J.-T., and McElroy, M. B.: Impacts of boundary layer mixing on pollutant vertical profiles in the lower troposphere: Implications to satellite remote sensing, Atmos. Environ., 44, 1726–1739, https://doi.org/10.1016/j.atmosenv.2010.02.009, 2010.

Liu, H., Liu, S., Xue, B., Lv, Z., Meng, Z., Yang, X., Xue, T., Yu, Q., and He, K.: Ground-level ozone pollution and its health impacts in China, Atmos. Environ., 173, 223–230, https://doi.org/10.1016/j.atmosenv.2017.11.014, 2018.

Liu, Y., and Wang, T.: Worsening urban ozone pollution in China from 2013 to 2017–Part 1: The complex and varying roles of meteorology, Atmos. Chem. Phys., 20, 6305-6321, https://doi.org/10.5194/acp-20-6305-2020, 2020.

Lu, X., Hong, J., Zhang, L., Cooper, O. R., Schultz, M. G., Xu, X., Wang, T., Gao, M., Zhao, Y., and Zhang, Y.: Severe Surface Ozone Pollution in China: A Global Perspective, Environ. Sci. Technol. Lett., 5, 487–494, https://doi.org/10.1021/acs.estlett.8b00366, 2018.

Lu, X., Zhang, L., Chen, Y., Zhou, M., Zheng, B., Li, K., Liu, Y., Lin, J., Fu, T.-M., and Zhang, Q.: Exploring 2016–2017 surface ozone pollution over China: source contributions and meteorological influences, Atmos. Chem. Phys., 19, 8339–8361, https://doi.org/10.5194/acp-19-8339-2019, 2019.

Lu, X., Zhang, L., Wang, X., Gao, M., Li, K., Zhang, Y., Yue, X., and Zhang, Y.: Rapid increases in warm-season surface ozone and resulting health impact over China since 2013, Environ. Sci. Technol. Lett., 7, 240–247, https://doi.org/10.1021/acs.estlett.0c00171, 2020.

Maji, K. J., Ye, W.-F., Arora, M., and Nagendra, S. M. S.: Ozone pollution in Chinese cities: Assessment of seasonal variation, health effects and economic burden, Environ. Pollut., 247, 792–801, https://doi.org/10.1016/j.envpol.2019.01.049, 2019.

Mao, J., Paulot, F., Jacob, D. J., Cohen, R. C., Crounse, J. D., Wennberg, P. O., Keller, C. A., Hudman, R. C., Barkley, M. P., and Horowitz, L. W.: Ozone and organic nitrates over the eastern United States: Sensitivity to isoprene chemistry, J. Geophys. Res. Atmos., 118, 11256–11268, https://doi.org/10.1002/jgrd.50817, 2013.

McLinden, C. A., Olsen, S. C., Hannegan, B., Wild, O., Prather, M. J., and Sundet, J.: Stratospheric ozone in 3-D models: A simple chemistry and the cross-tropopause flux, J. Geophys. Res., 105, 14653–14665, https://doi.org/10.1029/2000jd900124, 2000.

Mills, G., Sharps, K., Simpson, D., Pleijel, H., Broberg, M., Uddling, J., Jaramillo, F., Davies, W. J., Dentener, F., Van den Berg, M., Agrawal, M., Agrawal, S. B., Ainsworth, E. A., Buker, P., Emberson, L., Feng, Z., Harmens, H., Hayes, F., Kobayashi, K., Paoletti, E.,

and Van Dingenen, R.: Ozone pollution will compromise efforts to increase global wheat production, Glob. Chang. Biol., 24, 3560-3574, https://doi.org/10.1111/gcb.14157, 2018.

Mott, J. A., Mannino, D. M., Alverson, C. J., Kiyu, A., Hashim, J., Lee, T., Falter, K., Redd, S. C.: Cardiorespiratory hospitalizations associated with smoke exposure during the 1997 southeast Asian forest fires, Int. J. Hyg. Environ. Health., 208, 75–85, https://doi.org/10.1016/j.ijheh.2005.01.018, 2005.

Ni, R., Lin, J., Yan, Y., and Lin, W.: Foreign and domestic contributions to springtime ozone over China, Atmos. Chem. Phys., 18, 11447–11469, https://doi.org/10.5194/acp-18-11447-2018, 2018.

Ott, L. E., Pickering, K. E., Stenchikov, G. L., Allen, D. J., DeCaria, A. J., Ridley, B., Lin, R.-F., Lang, S., and Tao, W.-K.: Production of lightning NOx and its vertical distribution calculated from three-dimensional cloud-scale chemical transport model simulations, J. Geophys. Res., 115, D04301, https://doi.org/10.1029/2009JD011880, 2010.

Peterson, J. T., and Flowers, E. C.: Interactions between air pollution and solar radiation, Sol. Energy, 19, 23−32, https://doi.org/10.1016/0038-092X(77)90085-8, 1977.

Pye, H. O., Liao, H., Wu, S., Mickley, L. J., Jacob, D. J., Henze, D. K., and Seinfeld, J. H.: Effect of changes in climate and emissions on future sulfate-nitrate-mmonium aerosol levels in the United States, J. Geophys. Res., 114, D01205, https://doi.org/10.1029/2008JD010701, 2009.

Sherwen, T., Schmidt, J. A., Evans, M. J., Carpenter, L. J., Großmann, K., Eastham, S. D., Jacob, D. J., Dix, B., Koenig, T. K., Sinreich, R., Ortega, I., Volkamer, R., Saiz-Lopez, A., Prados-Roman, C., Mahajan, A. S., and Ordóñez, C.: Global impacts of tropospheric halogens (Cl, Br, I) on oxidants and composition in GEOS-Chem, Atmos. Chem. Phys., 16, 12239–12271, https://doi.org/10.5194/acp-16-12239-2016, 2016.

Shu, L., Wang, T., Han, H., Xie, M., Chen, P., Li, M., and Wu, H.: Summertime ozone pollution in the Yangtze River Delta of eastern China during 2013–2017: synoptic impacts and source apportionment, Environ. Pollut., 257, 113631, https://doi.org/10.1016/j.envpol.2019.113631, 2020

Sillman, S.: The relation between ozone, NOx and hydrocarbons in urban and polluted rural environments, Atmos. Environ., 33, 1821-1845, https://doi.org/10.1016/s1352-2310(98)00345-8, 1999.

Silver, B., Reddington, C. L., Arnold, S. R., and Spracklen, D. V.: Substantial changes in air pollution across China during 2015–2017, Environ. Res. Lett., 13, 114012, https://doi.org/10.1088/1748-9326/aae718, 2018.

Sekiya, T., and Sudo, K.: Roles of transport and chemistry processes in global ozone change on interannual and multidecadal time scales, J. Geophys. Res. Atmos., 119, 4903−4921, https://doi.org/10.1002/2013JD020838, 2014.

van der Werf, G. R., Randerson, J. T., Giglio, L., van Leeuwen, T. T., Chen, Y., Rogers, B. M., Mu, M., van Marle, M. J. E., Morton, D. C., Collatz, G. J., Yokelson, R. J., and Kasibhatla, P. S.: Global fire emissions estimates during 1997–2016, Earth Syst. Sci. Data, 9, 697–720, https://doi.org/10.5194/essd-9-697-2017, 2017.

Verstraeten, W. W., Neu, J. L., Williams, J. E., Bowman, K. W., Worden, J. R., and Boersma, K. F.: Rapid increases in tropospheric ozone production and export from China, Nat. Geosci., 8, 690–695, https://doi.org/10.1038/ngeo2493, 2015.

Wang, P., Yang, Y., Li, H., Chen, L., Dang, R., Xue, D., Li, B., Tang, J., Leung, L. R., and Liao, H.: North China Plain as a hot spot of ozone pollution exacerbated by extreme high temperatures, Atmos. Chem. Phys., 22, 4705–4719, https://doi.org/10.5194/acp-22-4705-2022, 2022.

Wang, T., Xue, L., Brimblecombe, P., Lam, Y. F., Li, L., and Zhang, L.: Ozone pollution in China: A review of concentrations, meteorological influences, chemical precursors, and effects, Sci. Total Environ., 575, 1582−1596, https://doi.org/10.1016/j.scitotenv.2016.10.081, 2017.

Xu, J., Ma, J. Z., Zhang, X. L., Xu, X. B., Xu, X. F., Lin, W. L., Wang, Y., Meng, W., and Ma, Z. Q.: Measurements of ozone and its precursors in Beijing during summertime: impact of urban plumes on ozone pollution in downwind rural areas, Atmos. Chem. Phys., 11, 12241–12252, https://doi.org/10.5194/acp-11-12241-2011, 2011.

Yang, Y., Liao, H., and Li, J.: Impacts of the East Asian summer monsoon on interannual variations of summertime surface-layer ozone concentrations over China, Atmos. Chem. Phys., 14, 6867-6880, http://doi:10.5194/acp-14-6867-2014, 2014.

Yang, Y., Zhou, Y., Li, K., Wang, H., Ren, L., Zeng, L., Li, H., Wang, P., Li, B., and Liao, H.: Atmospheric circulation patterns conducive to severe haze in eastern China have shifted under climate change, Geophys. Res. Lett., 48, e2021GL095011, https://doi.org/10.1029/2021GL095011, 2021.

Yang, Y., Li, M., Wang, H., Li, H., Wang, P., Li, K., Gao, M., and Liao, H.: ENSO modulation of summertime tropospheric ozone over China, Environ. Res. Lett., 17, 034020, https://doi.org/10.1088/1748-9326/ac54cd, 2022.

Yin, Z., Cao, B., and Wang, H.: Dominant patterns of summer ozone pollution in eastern China and associated atmospheric circulations, Atmos. Chem. Phys., 19, 13933–13943, https://doi.org/10.5194/acp-19-13933-2019, 2019.

Zhang, X., Zhao, L., Cheng, M., Wu, X., and Chen, D.: Urban ozone sink inferred from surface measurements in China, J. Clean. Prod., 253, 119881, https://doi.org/10.1016/j.jclepro.2019.119881, 2020.

Zhang, H., Wang, Y., Hu, J., Ying, Q., and Hu, X.-M.: Relationships between meteorological parameters and criteria air pollutants in three megacities in China, Environ. Res., 140, 242–254, https://doi.org/10.1016/j.envres.2015.04.004, 2015.

Zhao, Y., Zhang, K., Xu, X., Shen, H., Zhu, X., Zhang, Y., Hu, Y., and Shen, G.: Substantial changes in nitrogen dioxide and ozone after excluding meteorological impacts during the COVID-19 outbreak in mainland China, Environ. Sci. Technol. Lett., 7, 402−408, https://doi.org/10.1021/acs.estlett.0c00304, 2020.

Zhao, Z., and Wang, Y.: Influence of the West Pacific subtropical high on surface ozone daily variability in summertime over eastern China, Atmos. Environ., 170, 197–204, https://doi.org/10.1016/j.atmosenv.2017.09.024, 2017.

Zhou, D., Ding, A., Mao, H., Fu, C., Wang, T., Chan, L. Y., Ding, K., Zhang, Y., Liu, J., and Lu, A.: Impacts of the East Asian monsoon on lower tropospheric ozone over coastal South China, Environ. Res. Lett., 8, 044011, https://doi.org/10.1088/1748-9326/8/4/044011, 2013.

563   ***Code and data availability.*** The GEOS-Chem model is available at

564   https://zenodo.org/record/3974569#.YTD81NMzagR (last access: June 2023). O_3 observations

565   over China can be obtained at https://quotsoft.net/air (last access: June 2023). ERA5 reanalysis

566   data can be downloaded at https://www.ecmwf.int/en/forecasts/datasets/reanalysis-

567   datasets/era5 (last access: June 2023). The multi-model simulations of the Coupled Model

568   Intercomparison Project Phase 6 (CMIP6) are from https://esgf-node.llnl.gov/search/cmip6/

569   (last access: June 2023).

570   ***Author contribution***. YY designed the research; YY and YZ performed simulations and

571   analyzed the data. All authors including HW, LH, PW, and HL discussed the results and wrote

572   the paper.

573   ***Competing interests.*** At least one of the (co-)authors is a member of the editorial board of

574   Atmospheric Chemistry and Physics.

575   ***Acknowledgments.*** HW acknowledges the support by the U.S. Department of Energy (DOE),

576   Office of Science, Office of Biological and Environmental Research (BER), as part of the Earth

577   and Environmental System Modeling program. The Pacific Northwest National Laboratory

578   (PNNL) is operated for DOE by the Battelle Memorial Institute under contract DE-AC05-

579   76RLO1830.

580   ***Financial support.*** This study was supported by the National Natural Science Foundation of

581   China (grant 42293323), and the National Key Research and Development Program of China

582   (grant 2020YFA0607803), Jiangsu Science Fund for Distinguished Young Scholars (grant

583   BK20211541), ~~and the~~ Jiangsu Science Fund for Carbon Neutrality (grant BK20220031), and

584   the Graduate Research Innovation Project in Jiangsu province (KYCX23_1380).

585 **Table 1.** Anomalies in net rate of changes in tropospheric O_3 mass (Gg day^{-1}) over NCP (115°–
586 120°E, 38°–44°N), YRD (120°–125°E, 28°–32°N), SCB (102.5°–105°E, 30°–32°N) and PRD
587 (110°–115°E, 22°–26°N) due to physical and chemical processes in the most polluted months
588 (June 2018, July 2017, July 2015 and September 2019, respectively) relative to the same
589 months averaged during 1981–2019.
590

	Beijing	Shanghai	Chengdu	Guangzhou
Chemical reaction	2.36	2.38	-2.80	-1.52
Horizontal transport	1.58	−1.18	5.10	6.67
Diffusion and dry deposition	0.29	0.24	-0.73	-0.93

591
592

593 **Table 2.** Horizontal mass transport (Tg) of O_3 from the surface to 500 hPa over NCP (115°–
594 120°E, 38°–44°N), YRD (120°–125°E, 28°–32°N), SCB (102.5°–105°E, 30°–32°N) and PRD
595 (110°–115°E, 22°–26°N) areas in the severe polluted months (June 2018, July 2017, July 2015
596 and September 2019, respectively) and averaged over the same months of a year during 1981–
597 2019, as well as their differences. Positive values indicate incoming fluxes and negative values
598 indicate outgoing fluxes.

599

	Polluted month	Average	Anomalies
	NCP		
North	4.43	2.62	1.80
South	-2.22	-1.42	-0.81
East	-12.30	-11.31	-0.99
West	11.83	11.20	0.62
	YPD		
North	-4.13	-3.88	-0.25
South	3.58	3.20	0.37
East	-2.05	-3.90	1.85
West	2.03	4.04	-2.01
	SCB		
North	4.15	0.13	4.02
South	-2.30	0.48	-2.78
East	-1.10	-1.15	0.05
West	1.73	1.84	-0.11
	PRD		
North	2.70	0.72	1.97
South	-2.87	-0.90	-1.96
East	2.24	1.15	1.09
West	-2.32	-1.55	-0.76

600

601

602
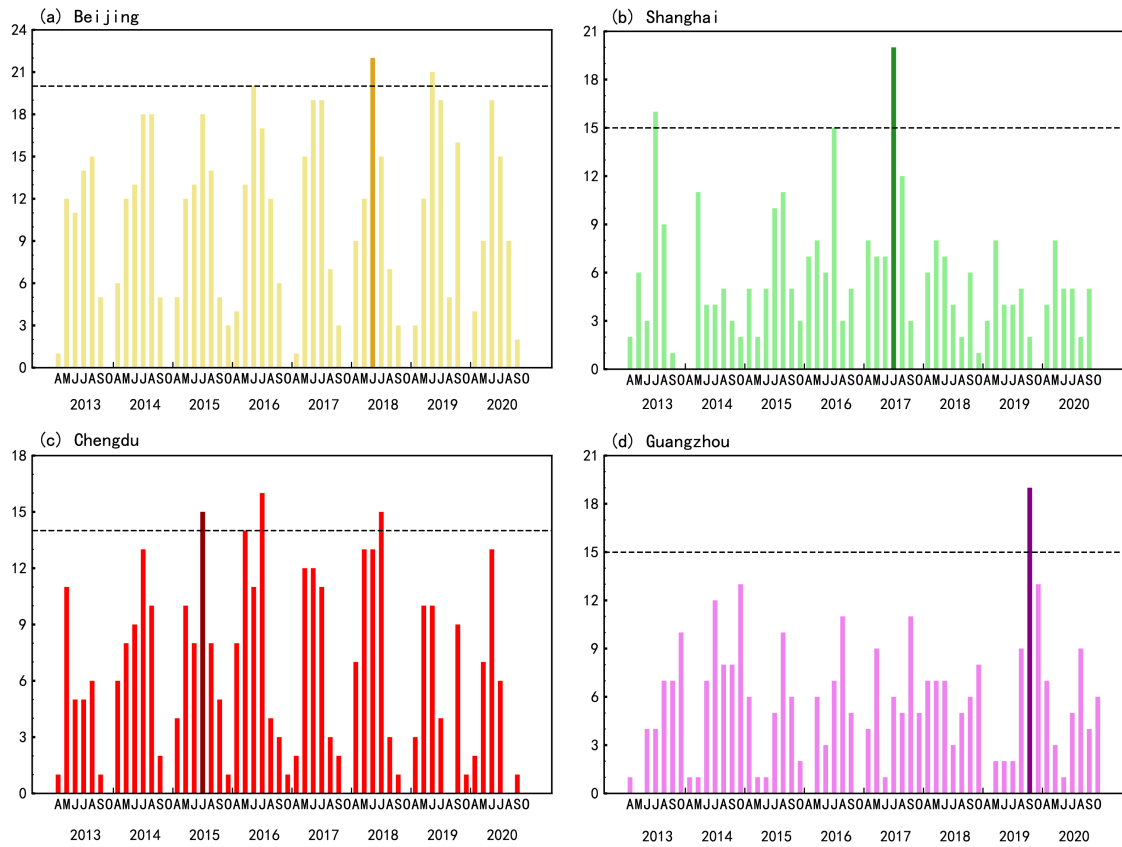
Figure 1. Time series of frequencies of severe O_3 pollution days (defined by daily maximum of 8-h average ozone (MDA8-O_3) concentration greater than 160 μg m^{-3}) in Beijing, Shanghai, Chengdu and Guangzhou (a–d) from April to October during 2013–2020. The dark-colored bars represent the most severe month (second most for Chengdu) that has the highest frequency of O_3 pollution days for the individual cities.

608
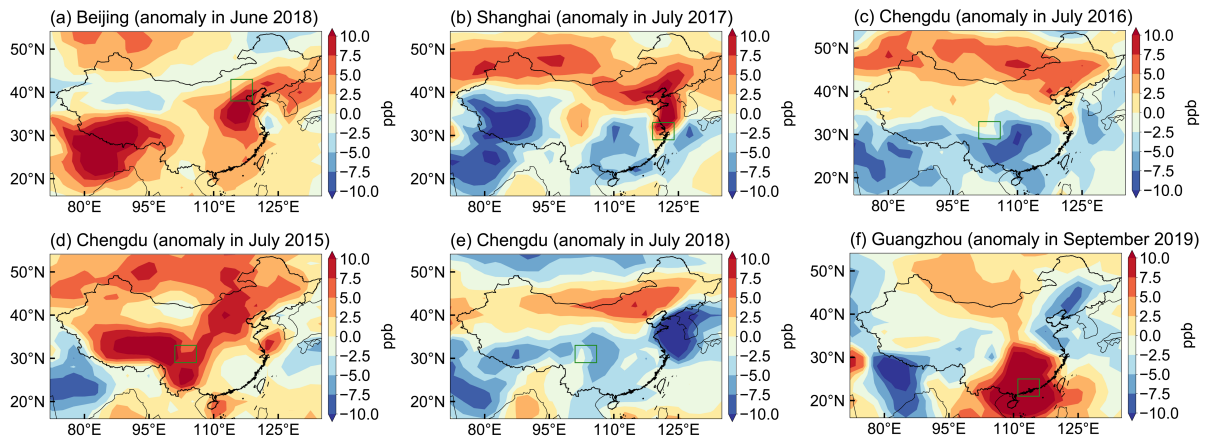
609

610 **Figure 2.** Spatial distribution of monthly O$_3$ concentration anomalies (part per billion, ppb) in
611 June 2018 (a), July 2017 (b), July 2016 (c), July 2015 (d), July 2018 (e) and September 2019
612 (f) relative to 40-year (1980–2019) monthly average for June (a), July (b, c, d, e) and September
613 (f), simulated in the GEOS-Chem model. The green boxes mark NCP (a), YRD (b), SCB (c, d,
614 e) and PRD (f).

615

616
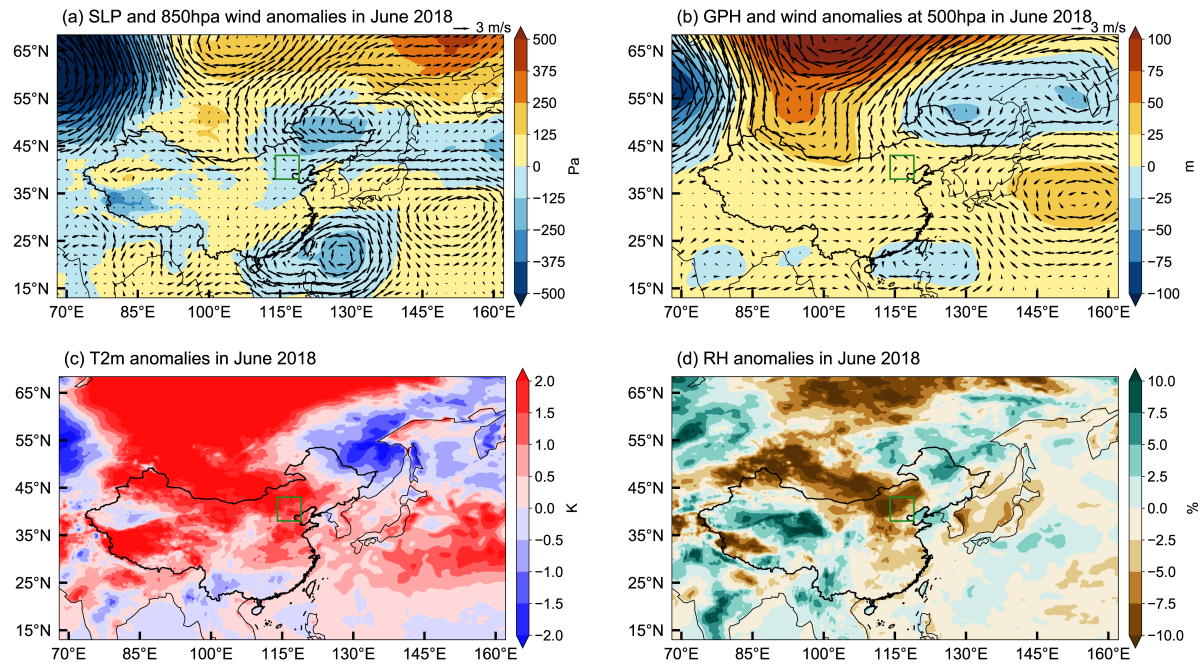
Figure 3. Anomalies in sea level pressure (SLP, Pa, shaded) and 850 hPa winds (m s^{-1}, vector)
(a), geopotential height (GPH, m, shaded) and winds at 500 hPa (m s^{-1}, vector) (b), 2-meter air
temperature (T2m, K) (c) and surface relative humidity (RH, %) (d) in June 2018 relative to
the 40-year (1980–2019) monthly average for June. The green boxes mark NCP.

621

622
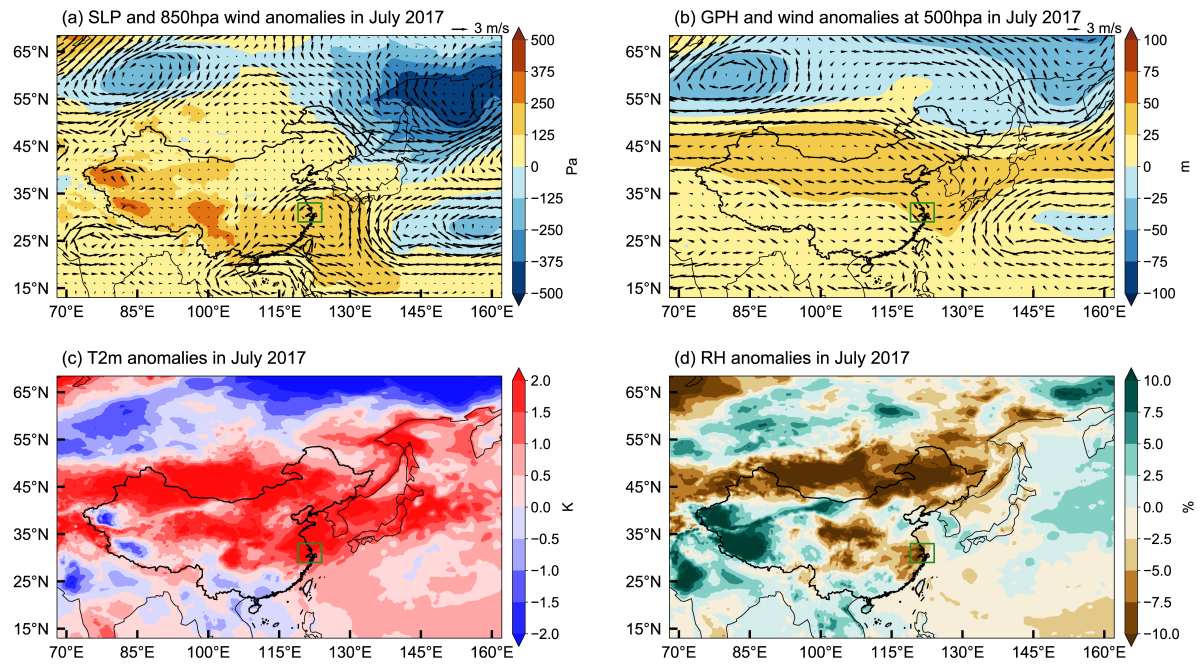
623 **Figure 4.** Same as Figure 3 but for the monthly anomalies in July 2017. The green boxes mark

624 YRD.

625

626
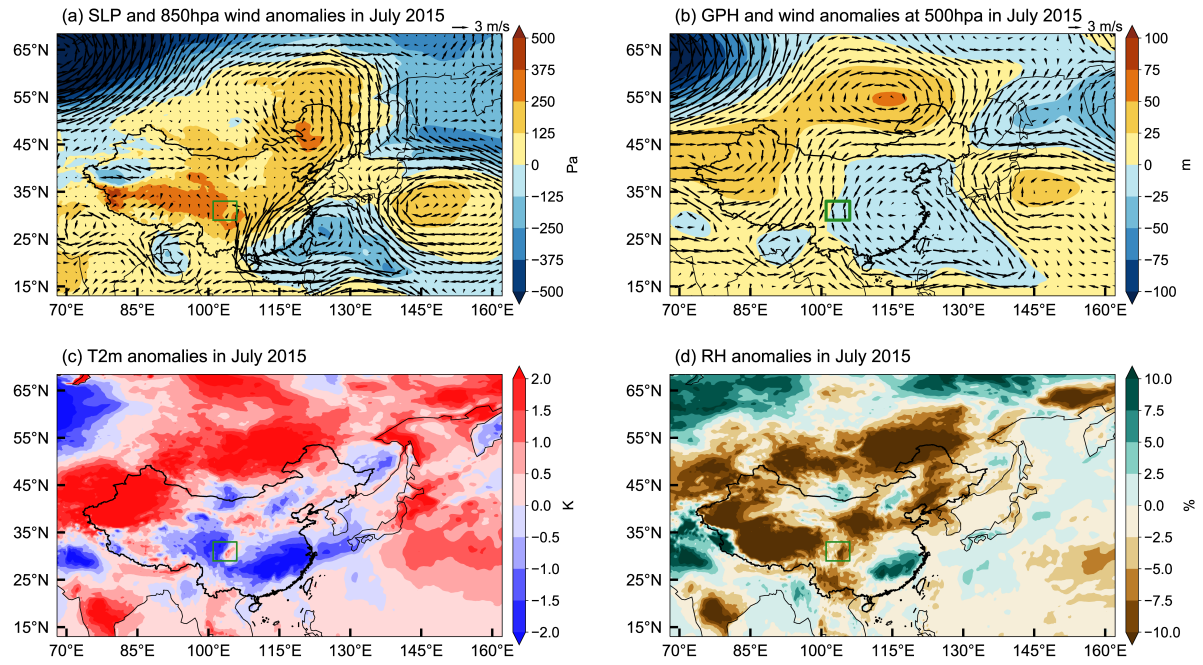
Figure 5. Same as Figure 3 but for the monthly anomalies in July 2015. The green boxes mark
SCB.

627
628
629

630
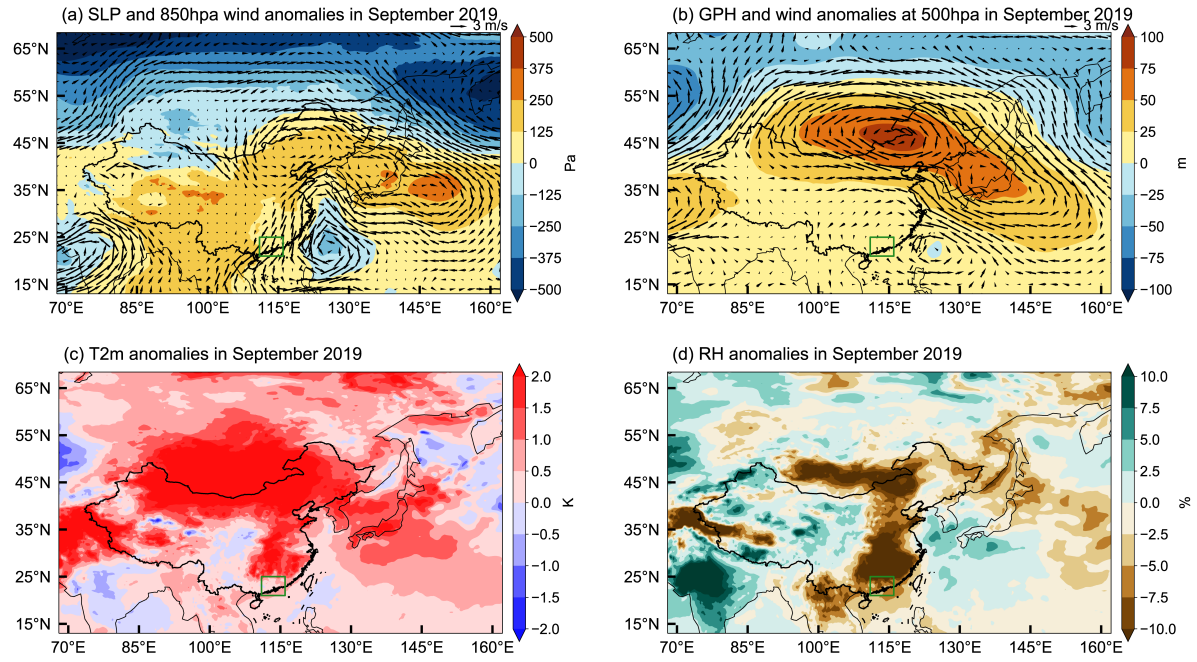
Figure 6. Same as Figure 3 but for the monthly anomalies in September 2019. The green boxes
mark PRD.
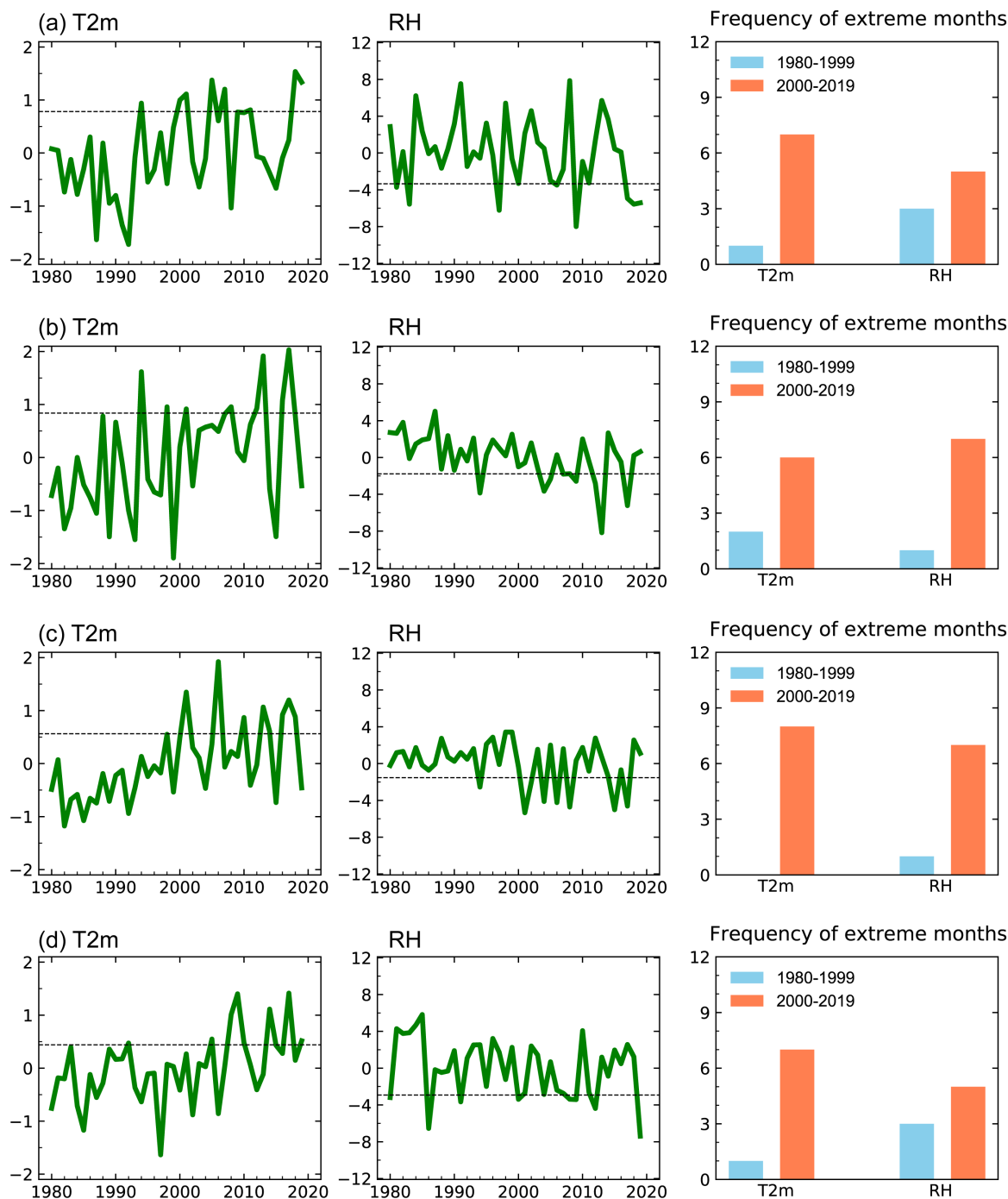
Figure 7. Time series of anomalies of T2m (K, left) and surface RH (%, middle) over (a) NCP (115°–120°E, 38°–44°N), (b) YRD (120°–125°E, 28°–32°N), (c) SCB (102.5°–105°E, 30°–32°N) and (d) PRD (110°–115°E, 22°–26°N) in the most polluted months during 1980–2019. The dotted lines mark the 80th percentile of the distributions for T2m and 20th percentile for RH. The bar charts (right) represent the frequency of T2m above the 80th percentile and RH anomalies below the 20th percentile during 1980–1999 (blue) and 2000–2019 (orange).

640
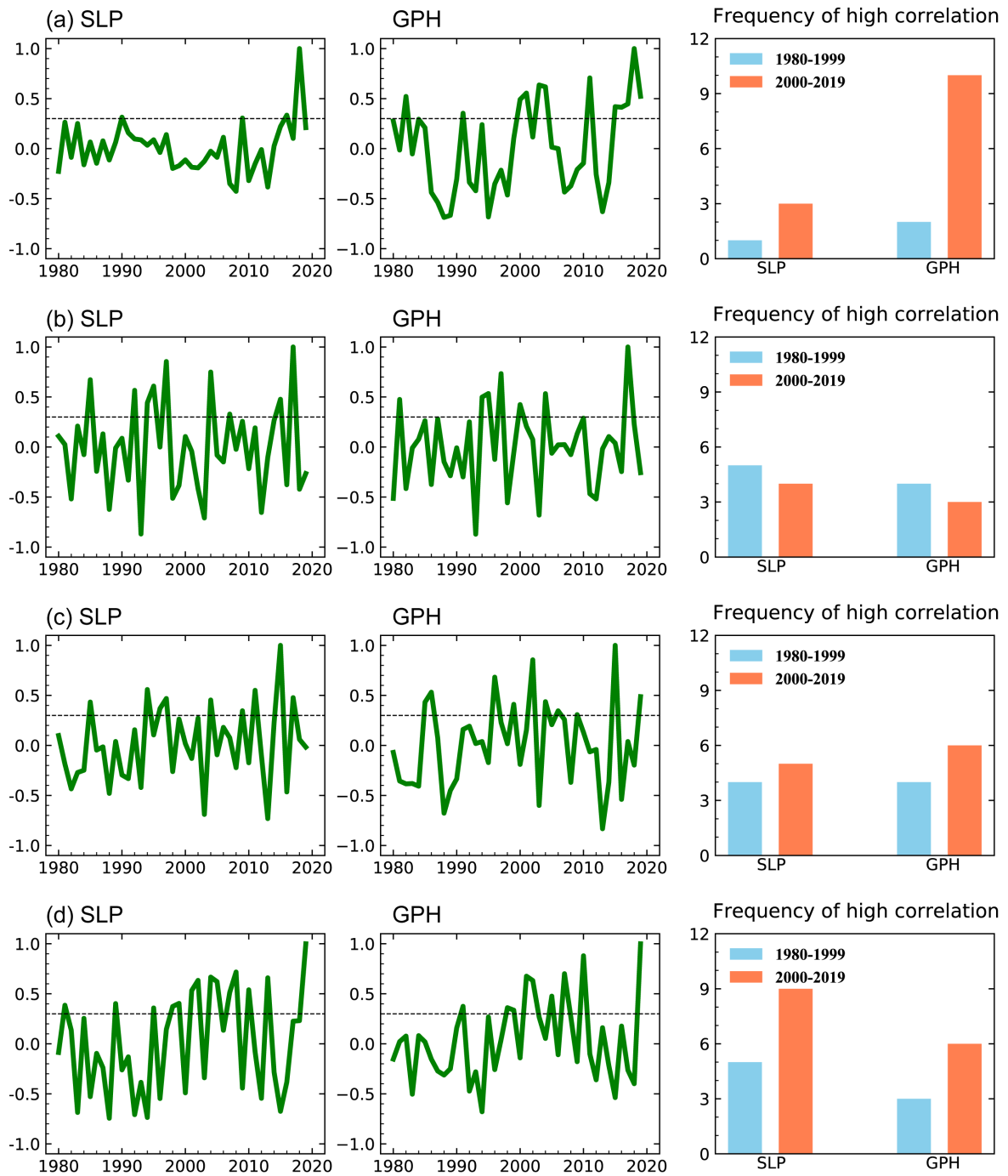
Figure 8. Time series of spatial correlation in SLP (left) and 500 hPa GPH (middle) anomalies
over East Asia and Western Pacific (EAWP, 90°–160°E, 20°–60°N) in June 2018 (a), July 2017
(b), July 2015 (c) and September 2019 (d) and those in the same targeted month of each year
during 1980–2019. The dotted lines mark the correlation coefficient of +0.3, which is used as
a threshold to define "moderate to high correlation". The bar chart (right) represents the
frequency of SLP and 500 hPa GPH anomalies in the same months during 1980–1999 (blue)
and 2000–2019 (orange) that have moderate to high correlation (>0.3) with those in June 2018,
July 2017, July 2015 and September 2019.

649
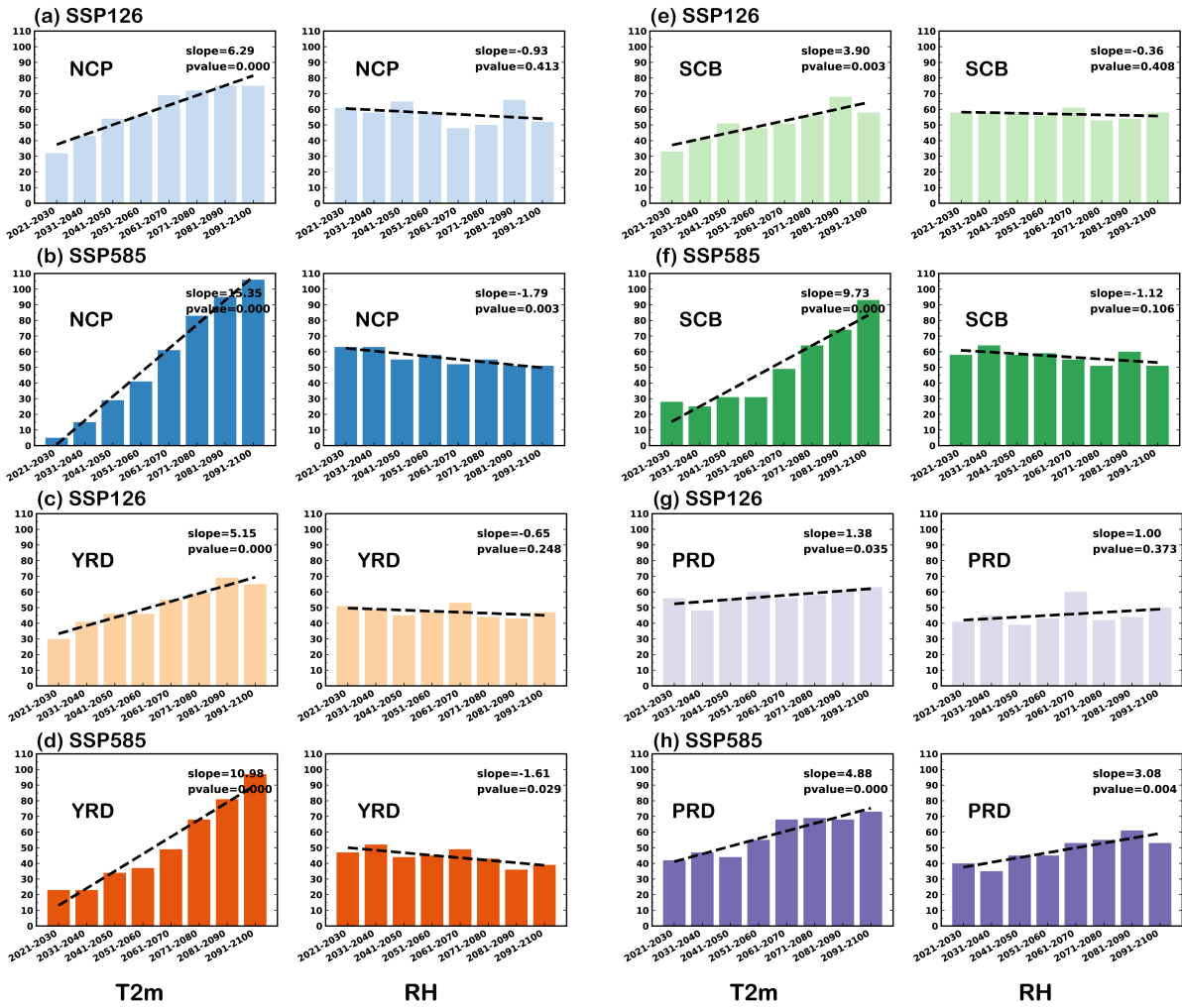
Figure 9. Frequencies of extreme months with T2m or RH anomalies exceeding the 80th percentile or below the 20th percentile of the distributions over NCP (115°–120°E, 38°–44°N) (a, b), YRD (120°–125°E, 28°–32°N) (c, d), SCB (102.5°–105°E, 30°–32°N) (e, f) and PRD (110°–115°E, 22°–26°N) (g, h) in each 10-year interval during 2021–2100 under two SSPs future scenarios of 13 CMIP6 models. The two SSPs are SSP1-2.6 and SSP5-8.5. The slope and P values of the linear regression during 2021–2100 are shown in the upper right of each panel.
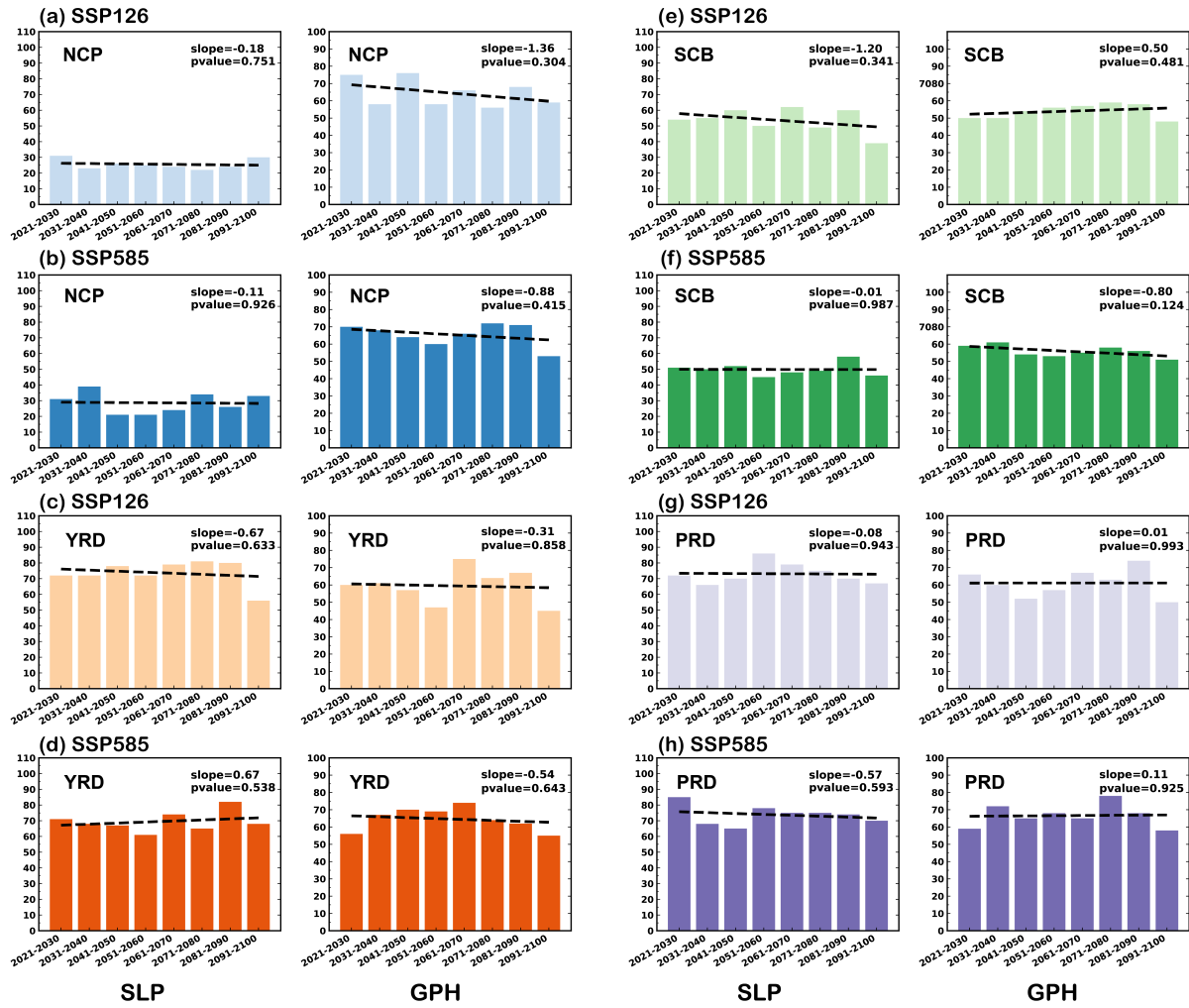
Figure 10. Frequencies of extreme months with SLP and 500 hPa GPH that have moderate to high correlation (>0.3) to those in June 2018 (a, b), July 2017 (c, d), July 2015 (e, f) and September 2019 (g, h) in each 10-year interval during 2021–2100 under two SSPs future scenarios of 13 CMIP6 models. The two SSPs are SSP1-2.6 and SSP5-8.5. The slope and P values of the linear regression during 2021–2100 are shown in the upper right of each panel. The linear trends of SLP and GPH in each model grid were removed before the correlation coefficient is calculated.